

FILE COPY  
NO. I-W

CASE FILE  
COPY

TECHNICAL MEMORANDUMS  
NATIONAL ADVISORY COMMITTEE FOR AERONAUTICS

---

No. 530

---

TRAVEL OF THE CENTER OF PRESSURE OF AIRFOILS  
TRANSVERSELY TO THE AIR STREAM

By Richard Katzmayr

From Berichte der Aeromechanischen Versuchsanstalt in Wien  
Volume I, No. 1, 1928

---

Washington  
September, 1929

**FILE COPY**

To be returned to  
the files of the National  
Advisory Committee  
for Aeronautics  
Washington, D. C.

NATIONAL ADVISORY COMMITTEE FOR AERONAUTICS.

TECHNICAL MEMORANDUM NO. 530.

TRAVEL OF THE CENTER OF PRESSURE OF AIRFOILS  
TRANSVERSELY TO THE AIR STREAM.\*

By Richard Katzmayr.

Knowledge of the resultant direction of the air force to the wing section is a prerequisite for airplane stability calculations. It is also indispensable for the distribution of the load on the different members of the wing structure. Since airplane wings have a limited span, a knowledge of the distribution of the air forces along the span is a second prerequisite, in addition to a knowledge of the pressure distribution along the chord. For the condition of minimum drag, the distribution along the span is elliptical. Tests with models and with full-sized wings show, however, that the elliptical distribution is rarely attained, the pressure distribution generally decreasing more gradually toward the wing tips, particularly at large angles of attack.

The experiments here described were performed for the purpose of obtaining the essential facts concerning the distribution of the air force along the span. We did not follow, however, the time-consuming method of point-to-point measurements

---

\*"Druckpunktswanderungen bei Flügeln quer zur Stromrichtung."  
From Berichte der Aeromechanischen Versuchsanstalt in Wien,  
Vol. I, No. 1 (1928), pp. 47-57.

of the pressure distribution on the wing surfaces (the method employed by American and English investigators in both model and free-flight tests), but determined directly the moment of the mean force about an axis passing through the middle of the span parallel to the direction of flight. The results thus obtained can be immediately used in strength calculations of wings and give values comparable to those obtained under the customary assumptions of an elliptical, rectangular, trapezoidal or other form of pressure decrease toward the wing tips. They also indicate the lateral travel of the center of pressure accompanying changes in the angle of attack. Lastly, they show how this lateral travel of the center of pressure is affected by changes in the aspect ratio, plan form, and thickness of the wing near the tips.

The proper performance of these tests necessitated the construction of special apparatus. As already mentioned, the object was to determine the point of application of the air force to each half of the wing with respect to an axis passing through the middle of the span parallel to the chord. Figure 1 shows the arrangement of the apparatus. It consists of a hanging weight  $P$  connected with the wing model by two fine steel wires 1 and 2. This weight enables the application of a variable horizontal force to the model in the direction of the arrow  $Q$  by shifting the support  $T$ . The magnitude of the pull  $Q_1$  can be determined by the formula  $Q_1 = Q_m / \sqrt{l^2 - m^2}$ , when  $Q$ ,  $l$  and  $m$

are known,  $Q$  being the total force exerted by the weight  $P$  at the point of suspension  $B$ ,  $l$  the length of the member  $BC$ , and  $m$  the deflection of the point  $B$  from its position of rest. Such pendulum balances have been repeatedly used in the Vienna laboratory for determining the forces exerted by airplane controls, the directional stability of airplanes, etc. They are simple, quick to set up, quite sensitive and accurate.

In order to enable the use of the pendulum balance in the contemplated tests, the wing models had to be cut in two at the middle of the span and perpendicularly to it. The two halves were then hinged together. The hinge had to perform three tasks. Its first task was to hold the two parts together with as little friction as possible. Its second task was to carry the points of attachment for rendering the model immovable in the wind tunnel. Lastly, it had to support a device to indicate whether the pulls  $Q_1/2$  were in equilibrium with the air forces on the two halves of the model. The hinge consisted of three metal parts  $a$ ,  $b$  and  $c$  (Fig. 2), the middle one ( $b$ ) being rigidly attached to one-half of the model, and the other two ( $a$  and  $c$ ) to the other half. The three metal parts were twice drilled lengthwise, the axes of the holes being parallel and 40 mm (1.57 in.) apart. The hole near the upper side of the wing served to receive the steel hinge pin  $d$ , which fitted tightly in the end parts  $a$  and  $c$  but loosely in the middle part  $b$ , so that the latter could move easily. A steel pin  $e$

could likewise be stuck through the second hole near the lower surface of the wing, thus rigidly locking the hinge. The easiest possible operation of the hinge was obtained by inserting thin washers between the three parts, around the hinge pin, so that the edges of the hinge parts did not come into contact with one another. The upper point of attachment of the model was provided by fastening a fork *f* to the upper end of the hinge pin *d*. The fork had a hole *g* through which a steel wire was passed to form a flexible union with the upper support *u* (Fig. 1), which was connected with the lift balance in the usual manner. The two lower supports *v* and *w* of the lift balance were replaced by fine steel wires attached to the rod *i* by means of the hole *h*. In order to keep the wires *v* and *w* continually taut, a third wire *o* was led to the bell crank *d* carrying the counterweight  $Q_2$ . The angle of attack could be varied in the usual manner with the aid of the supports *u*, *v* and *w*. Moreover, the model was suspended from the drag balance by the wire *r*, which was also attached to the fork *f* through the hole *g*. The wires *s* and *t*, which likewise led to the drag balance, were left slack and served as a safety suspension in case the wire *r* should break. This method of suspension made it possible to move the wing halves back and forth about the hinge pin *d*, despite the rigid mooring of the latter and, consequently, of the model in the air stream. The hinge was attached to the wing halves in such a way that the center of the

hole  $g$  in the fork  $f$  lay in the leading edge of the model and the line connecting  $g$  and  $h$  lay in the chord. This line was also parallel to the hinge pin  $d$  (Fig. 2).

A brass bar  $k$  was firmly screwed to the middle part  $b$  of the hinge. When the hinge was closed, there was a space of about 1 mm (0.04 in.) between this bar and the other two parts  $a$  and  $c$  of the hinge. This bar served as a stop. To the wooden model there was screwed a brass angle  $m$  carrying a set screw which could be screwed against the bar  $k$ . This bar and the angle  $n$  were connected with a galvanometer through two wires and a four-volt storage battery. If the bar and the screw of the angle  $n$  came in contact, the galvanometer needle was deflected. This device served as an indicator of the state of equilibrium between the air force which tended to open the wing halves about the hinge and the pull  $Q_1$  of the pendulum balance which tended to close them. Figure 3 shows the hinge and the contact device mounted on the wing.

In order that changing the angle of attack would cause no motion of the wing halves about the hinge pin, the three suspension points  $E$ ,  $F$  and  $G$  (Fig. 1) were arranged in a straight line. It is obvious that the weight of the model exerted a moment about the hinge axis which had to be offset by a corresponding component of the pull of the pendulum balance, in order to maintain equilibrium at different angles of attack. This gravity component had to be determined therefore in still

air before the power was turned on and then subtracted from the results obtained in the air stream.

The dimensions of the hinge and the distribution of the screws were such that the same hinge could be used for all the different models. On wide models, however, there was a 10 mm (0.4 inch) slot between the wing halves at the back end of the hinge (Fig. 3). In order to avoid any error in the distribution of the air pressure in the middle of the span, thin silk paper was pasted over this slot before the tests were made. Since the paper was not very stiff, there was no danger of its hampering the mobility of the wing halves.

After it appeared probable that the results depended also on the aspect ratio of the wings, rectangular wing models of the following dimensions were tested: 1210 x 120, 970 x 120, 730 x 120, 610 x 120 (Figs. 5-8), 1210 x 200, 810 x 200, and 410 x 200 mm (Figs. 9-11), the aspect ratios therefore, being respectively, 10.08, 8.08, 6.08, 5.08, 6.05, 4.05, and 2.05. Tests were also made with a trapezoidal wing which, by cutting, was given spans of 1210, 810 and 405 mm (Figs. 12-15), the aspect ratios therefore being respectively, 6.8, 5.13, and 1.84. Lastly, we tested a wing of common form in practice, consisting of a rectangular middle piece to each end of which a trapezoidal end piece was joined. The span of this model was 1210 mm. Figure 4 shows the shape of the wing section or profile, which was the same for all the models, includ-

ing the trapezoidal ones in which the thickness was kept proportional to the diminishing chord.

The test results are given in Tables I-XI and Figures 16-18. In addition to the usual data  $2 c_A$ ,  $2 c_W$  and  $2 c_M$ , the center-of-pressure coordinates  $e$  and  $z$ , are given. The former is the distance in millimeters of the intersection of the aerodynamic resultant with the wing chord from the leading edge of the wing. The latter is the distance of the air force on a half-wing from the center of the span, measured perpendicularly to the direction of flow. For trapezoidal wings  $2 c_M$  is referred to an axis 10 mm (0.4 in.) behind the leading edge. The distance  $e$  is also measured from the same reference line. With the aid of the coordinates  $e$  and  $z$ , it is possible to draw the curve obtained by joining the points of application of the air-force vectors on a half-wing in the plane of the chord for different angles of attack (Figs. 5-15).

These curves show that, with increasing angle of attack  $\alpha$ , the center of pressure moves toward the wing tip. On small rectangular wings, this transverse travel is greater in proportion to the span, for small aspect ratios than for large ones. The reverse is the case for large rectangular wings. For small aspect ratios, moreover, the center of pressure lies nearer the wing tip at small angles of attack than at medium ones. For the rectangular wing with the smallest tested aspect ratio of 2.05, this phenomenon is reversed in that the air



force again travels toward the middle of the span with increasing angle of attack. The results show, however, that they are affected by the magnitude of the index value. In fact, not quite doubling the index value has the same effect on the transverse travel of the center of pressure as a diminution of the aspect ratio. These remarks apply to rectangular wings. The phenomena are generally similar for trapezoidal wings. With the latter, a reduction in the aspect ratio diminishes the travel of the center of pressure, as is the case with large rectangular wings. Direct comparison of the three trapezoidal wings is not possible, however, because the results (due to the different chords of the three models) are based on different index values. The wing with the combination plan form (Fig. 15) shows the greatest relative transverse travel of the center of pressure, amounting to 17% of the span, but behaves very much like the other wings in other respects.

Moreover, the results show that, for the ordinary angles of attack, aspect ratios and wing shapes, the path of the aerodynamic force very closely follows a parallel to the air flow passing through the center of gravity of the half-wing. These centers of gravity  $S$  are also indicated in Figures 5 to 15. With large aspect ratios and large angles of attack, the travel of the center of pressure toward the wing tip is no longer negligible. This travel increases with increasing index values.

TABLE I.

Wing 1.  
 $s/t = 1210/120$  mm  
 Area = 1412 cm<sup>2</sup>  
 Rectangular,  $\lambda = 10.09$   
 $p = 30$  mm water pressure

$\alpha$	$2 c_A$	$2 c_W$	$2 c_M$	e	z
-3	15.1	3.00	14.9	171.0	274.5
0	38.5	2.97	19.8	82.6	304
3	55.8	4.07	23.4	61.0	289
6	76.0	5.38	27.6	52.2	298
9	91.1	7.11	30.8	45.0	298
12	104.0	9.25	33.6	42.6	308
15	111.5	12.75	35.0	40.25	330
18	111.0	18.90	36.8	41.0	354
21	81.4	27.20	38.3	42.4	-

TABLE II.

Wing 2  
 $s/t = 970/120$  mm  
 Area = 1164 cm<sup>2</sup>  
 Rectangular,  $\lambda = 8.09$   
 $p = 30$  mm water pressure

$\alpha$	$2 c_A$	$2 c_W$	$2 c_M$	e	z
-3	13.0	3.04	13.74	128.0	177.5
0	32.9	3.12	17.60	64.9	224
3	52.0	3.90	22.05	51.4	225
6	71.0	5.38	26.07	46.15	235
9	88.5	7.63	30.5	41.8	234
12	100.5	10.25	33.0	39.8	251.5
15	107.5	12.82	34.8	39.2	260.5
18	107.5	19.70	36.5	41.05	280.5
21	72.8	26.25	39.7	56.6	360

TABLE III.

Wing 3  
 $s/t = 730/120$  mm  
 Area = 876 cm<sup>2</sup>  
 Rectangular,  $\lambda = 6.09$   
 $p = 30$  mm water pressure

$\alpha$	$2 c_A$	$2 c_W$	$2 c_M$	$e$	$z$
-3	12.73	3.25	12.9	123.1	155.1
0	31.20	3.35	17.1	66.6	158
3	48.70	4.28	21.3	53.5	181
6	68.30	6.24	25.9	46.05	179.2
9	83.30	7.99	29.55	43.15	178.5
12	96.0	10.88	32.6	39.7	177
15	101.8	14.13	34.1	40.9	183.5
18	96.0	20.20	34.7	44.0	194.6
21	84.5	27.20	39.3	47.3	236

TABLE IV.

Wing 4  
 $s/t = 610/120$  mm  
 Area = 733 cm<sup>2</sup>  
 Rectangular,  $\lambda = 5.09$   
 $p = 30$  mm water pressure

$\alpha$	$2 c_A$	$2 c_W$	$2 c_M$	$e$	$z$
-3	12.3	3.28	15.0	146.8	175.5
0	30.0	3.41	17.45	69.9	144
3	47.8	3.96	21.4	54.0	151
6	64.1	5.60	25.5	47.7	150.4
9	80.5	7.65	29.0	43.4	152
12	90.8	10.63	31.35	41.5	158.5
15	98.31	14.05	33.4	44.3	166.3
18	101.0	19.65	33.55	49.7	170
21	77.8	27.0	34.5	53.5	214

TABLE V.

Wing 5  
 $s/t = 1210/200$  mm  
 Area = 2420 cm<sup>2</sup>  
 Rectangular,  $\lambda = 6.05$   
 $p = 30$  mm water pressure

$\alpha$	$2 c_A$	$2 c_W$	$2 c_M$	$e$	$z$
-9	8.27	2.25	13.4	324.0	450
-6	25.6	2.32	17.1	133.3	310
-3	43.8	3.06	21.2	97.0	277.5
0	61.6	4.63	25.4	82.5	271.5
3	78.2	6.45	29.3	75.0	262
6	93.0	8.89	33.6	72.2	267
9	107.0	11.55	36.1	67.5	265.5
12	113.3	14.87	38.8	68.0	283
15	117.8	19.22	39.5	67.0	299
18	117.8	23.95	41.4	70.9	321
21	117.0	28.10	41.8	71.5	333
24	111.5	31.80	42.7	76.5	346

TABLE VI.

Wing 6  
 $s/t = 810/200$  mm  
 Area = 1620 cm<sup>2</sup>  
 Rectangular,  $\lambda = 4.05$   
 $p = 30$  mm water pressure

$\alpha$	$2 c_A$	$2 c_W$	$2 c_M$	$e$	$z$
-9	4.94	2.285	13.32	-	-
-6	20.05	2.47	16.3	162.5	210
-3	35.8	3.34	20.0	111.8	207
0	51.6	4.70	23.7	92.0	198
3	68.0	6.60	27.4	80.6	197
6	83.4	9.26	31.76	74.6	192.5
9	95.6	12.22	34.8	72.9	190.2
12	104.0	15.4	36.83	70.7	189.2
15	109.5	20.5	37.24	69.8	184.9
18	109.5	25.6	38.16	69.6	187
21	103.6	30.2	38.16	73.5	198.5
24	102.0	34.2	40.9	90.7	201.3

TABLE VII.

Wing 7  
 $s/t = 410/200$  mm  
 Area = 820 cm<sup>2</sup>  
 Rectangular,  $\lambda = 2.05$   
 $p = 30$  mm water pressure

$\alpha$	$2 c_A$	$2 c_W$	$2 c_M$	e	z
-9	2.44	2.94	12.76	-	-
-6	13.42	2.99	14.0	208.8	89.2
-3	25.6	3.5	16.4	128.0	94.6
0	38.4	4.76	19.0	104.0	94.9
3	50.6	6.35	21.8	86.4	95.3
6	63.5	8.91	25.0	78.9	93.1
9	76.3	12.2	27.95	73.0	90.4
12	88.5	16.0	31.3	70.9	86.4
15	95.8	19.3	34.6	72.4	86.6
18	101.0	24.15	37.2	73.5	83.5
21	101.0	27.8	38.0	75.15	83.5
24	92.7	34.9	39.9	86.2	90.9

TABLE VIII.

Wing 8  
 $s/t_m = 1210/180$  mm  
 Area = 2184 cm<sup>2</sup>  
 Trapezoidal,  $\lambda = 6.72$   
 $p = 30$  mm water pressure

$\alpha$	$2 c$	$2 c$	$2 c$	e	z
-9	5.05	2.515	12.2	-	-
-6	24.22	2.58	16.42	-	-
-3	41.6	3.25	20.03	200.0	176.5
0	58.6	4.49	24.21	125.8	165.0
3	75.3	5.92	27.8	103.2	204.0
6	96.7	8.15	32.35	89.3	206.5
9	103.9	10.52	34.0	85.6	228.2
12	115.7	13.5	36.81	78.4	232.5
15	125.0	17.02	39.2	72.0	242
18	118.5	22.2	41.8	69.7	283
-	-	-	-	-	-
-	-	-	-	-	-

TABLE IX.

Wing 9  
 $s/t_m = 405/220$  mm  
 Area = 891 cm<sup>2</sup>  
 Trapezoidal,  $\lambda = 1.15$   
 $p = 30$  mm water pressure

$\alpha$	$2 c$	$2 c$	$2 c$	$e$	$z$
-9	2.8	4.01	11.4	-	-
-6	12.9	4.04	13.01	222	-
-3	24.7	4.32	14.86	132.8	65.5
0	36.5	5.50	17.12	103.6	77.5
3	47.1	7.3	19.73	94.5	84.6
6	58.4	10.1	22.5	85.0	89.0
9	68.6	12.9	25.32	80.15	93.0
12	80.8	16.85	28.8	78.5	94.0
15	90.0	20.85	32.05	77.0	94.5
18	95.4	25.22	35.6	82.4	96.0
21	95.4	29.2	36.5	84.1	86.8

TABLE X.

Wing 10  
 $s/t_m = 810/160$  mm  
 Area = 1296 cm<sup>2</sup>  
 Trapezoidal,  $\lambda = 5.05$

$\alpha$	$2 c_A$	$2 c_W$	$2 c_M$	$e$	$z$
-9	2.315	3.16	10.18	-	-
-6	18.5	3.09	13.67	-	180
-3	35.5	3.7	17.2	77.6	179.2
0	51.5	4.86	21.55	66.75	185.7
3	68.0	6.49	25.7	60.7	188.1
6	85.0	8.8	30.4	57.4	182.1
9	99.5	11.1	33.9	54.6	178.8
12	114.1	14.1	37.1	52.0	175.0
15	126.5	17.35	40.0	57.15	175.0
18	132.7	21.3	42.6	58.05	172.0
21	125.0	27.4	44.9	57.9	180.0

$p = 30$  mm water pressure

TABLE XI.

Wing 11  
 $s/t_m = 1210/160$  mm  
 Area = 2100 cm<sup>2</sup>  
 Rectangular and Trapezoidal,  $\lambda = 7.56$   
 $p = 30$  mm water pressure

$\alpha$	$2 c_A$	$2 c_W$	$2 c_M$	e	z
-9	6.66	2.24	12.8	-	-
-6	24.78	2.34	14.5	135.6	190.0
-3	44.7	3.05	20.5	93.3	224.7
0	63.4	4.29	24.6	79.0	236.4
3	81.0	6.14	28.8	72.4	243.2
6	95.2	8.32	32.2	70.5	252.5
9	108.0	11.16	35.6	66.5	266.1
12	115.6	14.3	36.8	64.3	280.2
15	117.0	17.9	39.3	72.7	303.2
18	117.0	23.6	41.8	72.7	316.0
21	115.6	28.0	41.5	88.0	333.0
24	96.1	33.8	-	-	396.0

Translation by Dwight M. Miner,  
 National Advisory Committee  
 for Aeronautics.

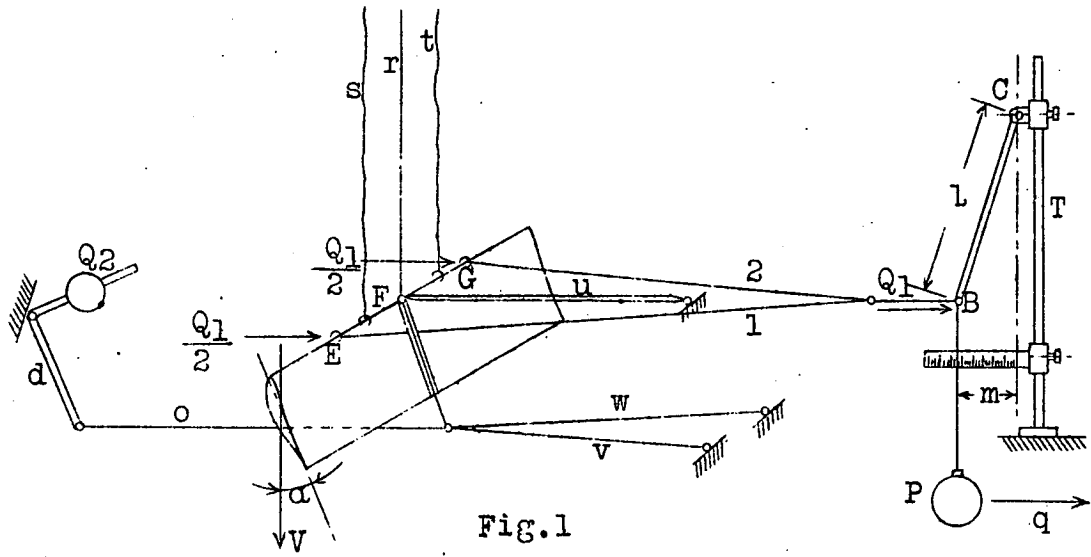


Fig.1

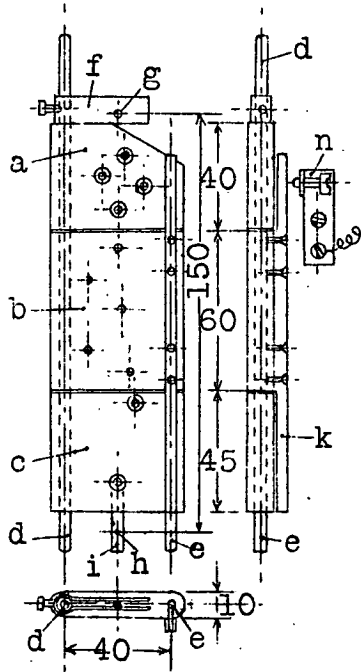


Fig.2

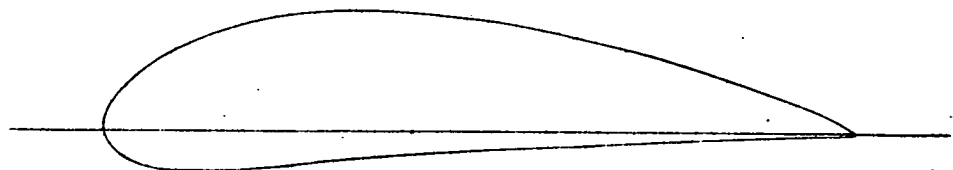


Fig.4



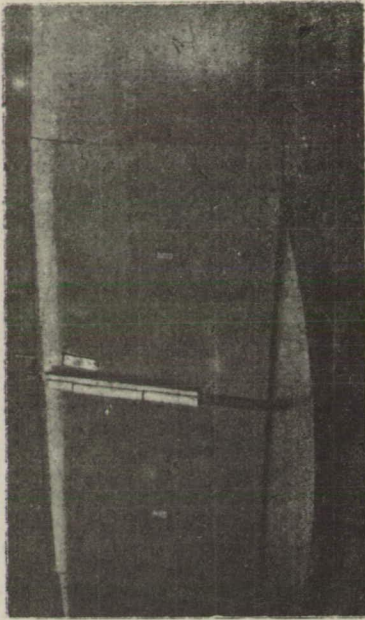


Fig.3

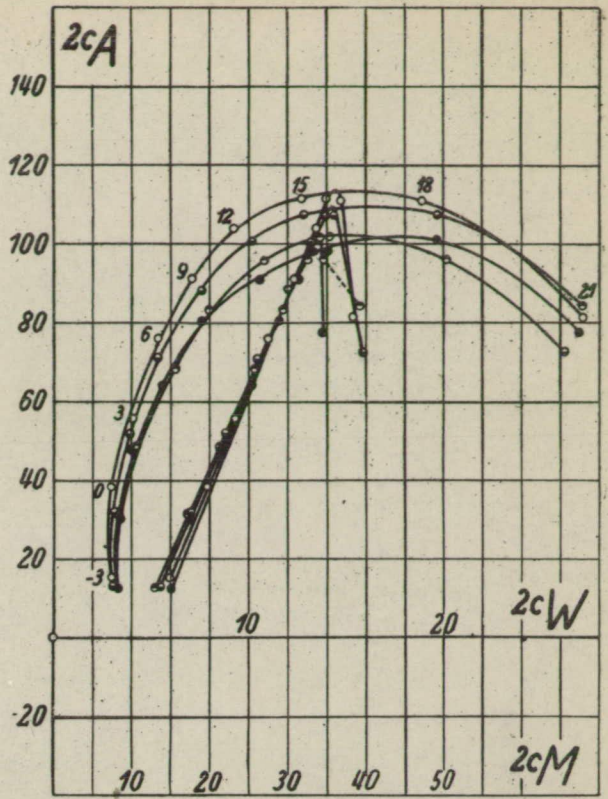


Fig.16

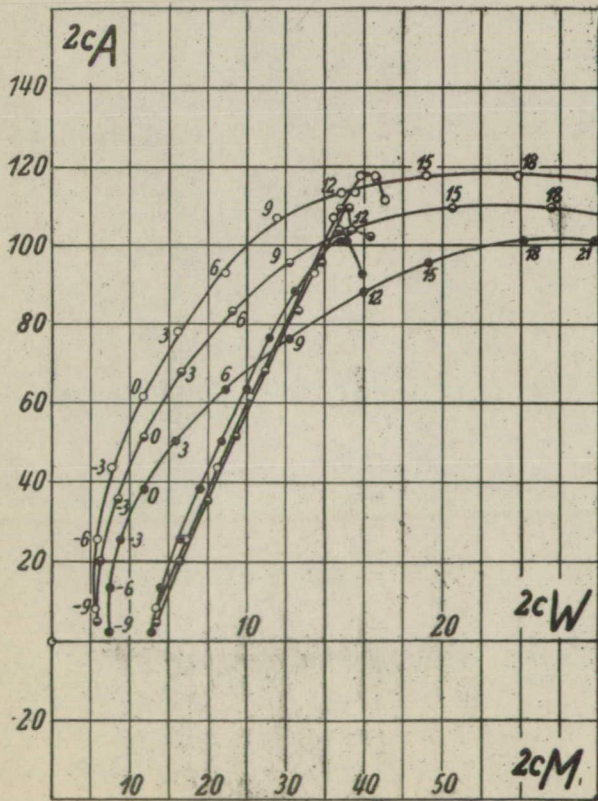


Fig.17

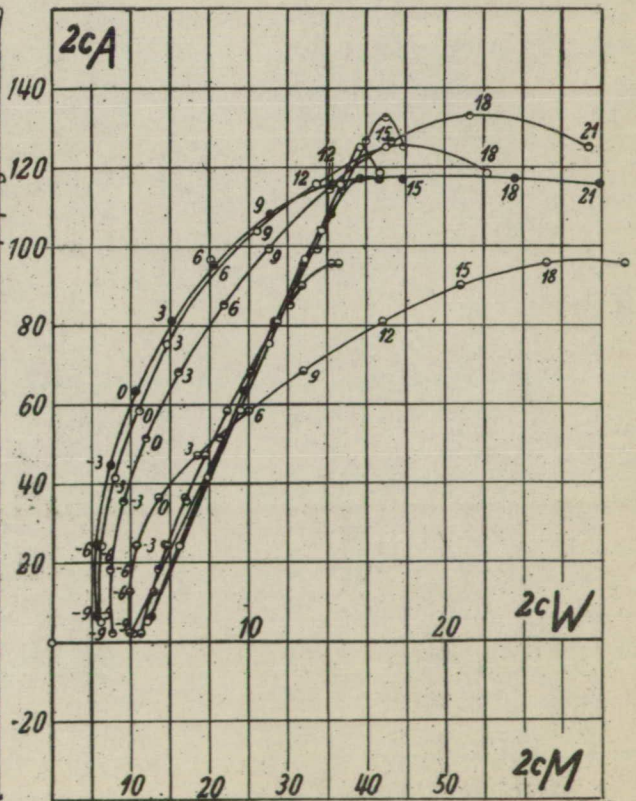
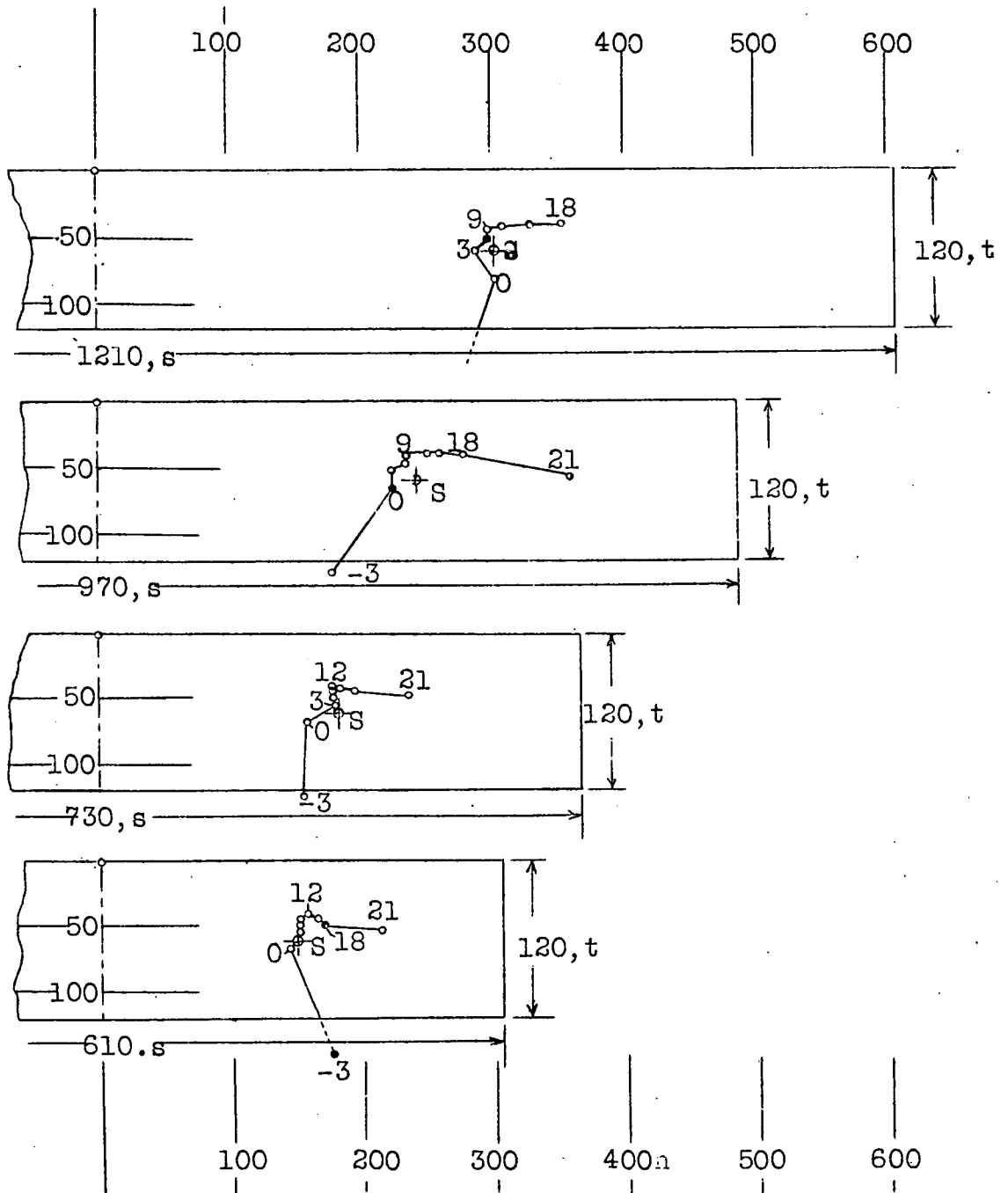
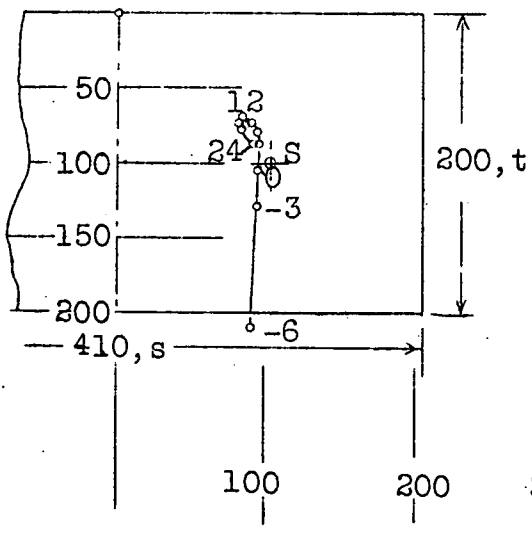
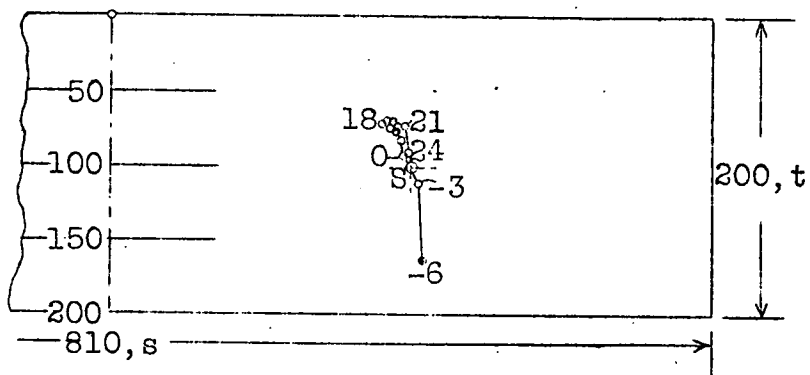
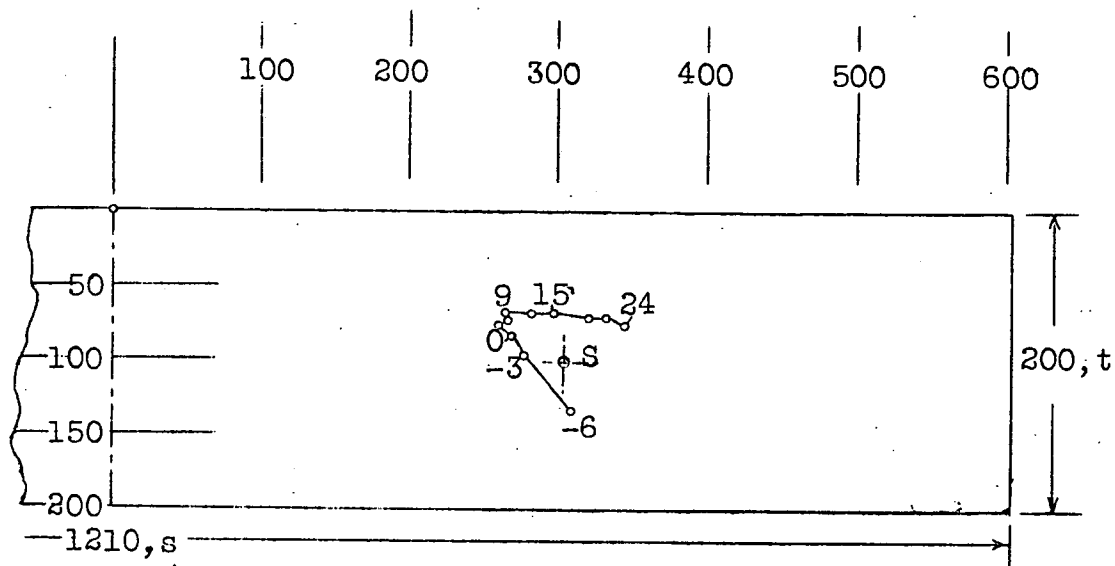


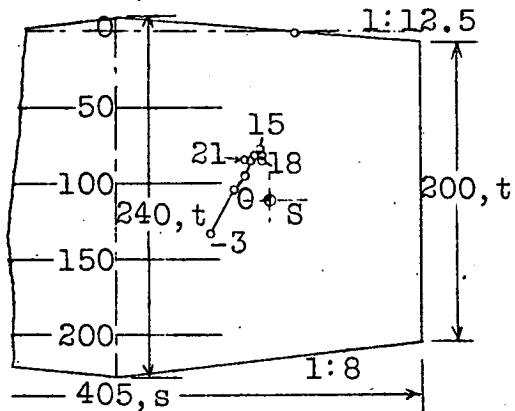
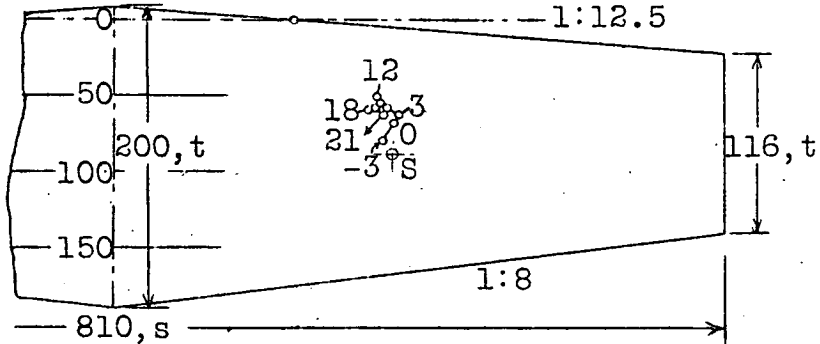
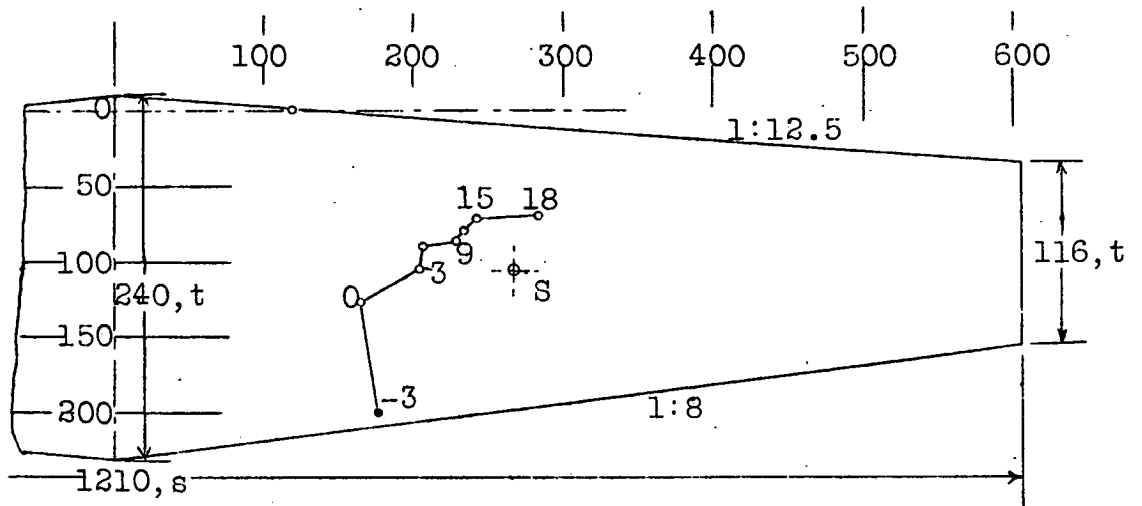
Fig.18



Figs.5,6,7,8.



Figs. 9, 10, 11.



Figs. 12, 13, 14, 15.

